A NOVEL APPROACH TO ESTIMATE SOIL MOISTURE UNDER VEGETATION USING PARTIAL POLARIMETRIC ALOS PALSAR DATA

C. N. Koyama [a, *], K. Schneider [a]

[a] Dept. of Geography, University of Cologne, Albertus-Magnus-Platz, 50923 Cologne, Germany – (christian.koyama, karl.schneider)@uni-koeln.de

Commission VIII, Working Group VIII/4

KEY WORDS: SAR, ALOS, Polarization, Vegetation, Soil, Surface Roughness, Estimation

ABSTRACT:

A major impediment to accurate quantitative retrievals of soil moisture from SAR is the disturbing effect caused by vegetation and surface roughness. With most operational space borne systems it is not possible to separate the different scattering contributions of the soil and vegetation components. In this paper we use the coherent-on-receive dual-polarized standard acquisitions (FBD343) of PALSAR aboard the Advanced Land Observing Satellite (ALOS "Daichi") acquired over an arable land test site in Western Germany. By applying a PolSAR decomposition technique, namely the H/A/Alpha decomposition, we exploit the phase information to increase the amount of observables. The potential to derive information on biomass and surface roughness from the dual-pol data is investigated based on correlation analyses between PALSAR observables and in situ measurements. High sensitivities towards surface roughness and crop biomass could be ascertained. Using these findings, we estimate surface roughness *ks* and sugar beet total wet weight with RMS errors of 0.11 and 2.66 kg/m², respectively. The good quality of the estimates allows correcting the backscattering coefficients for the surface roughness effects. In a first test the accuracy of soil moisture retrievals on bare soil could be increased from 4.5 to 3.6 Vol.-% using the roughness correction. Our findings give a promising outlook in terms of the possibility to develop an operational soil moisture retrieval model for PALSAR data collected in the FBD mode.

1. INTRODUCTION

Information on the spatial and temporal distribution of soil water contents at the land surface is of high importance for land applications such as hydrology, agriculture and meteorology. SAR systems have proven their potential to quantitatively estimate near surface volumetric soil moisture at high spatial resolution. However, to date their use has been generally limited and still no operational retrieval algorithm is available. Besides the surface roughness, a major impediment to accurate quantitative retrievals of soil moisture is the presence of a vegetation cover which is characterized by gradual variations over the growing season. Both factors modulate the radar sensitivity to soil dielectric constant rendering accurate soil moisture retrieval intricate to achieve. Since for a single-channel SAR (e.g. ERS-1/2, JERS, RADARSAT-1, etc.) there exist many combinations of surface parameters mapping the same SAR observable, it is not possible to separate the different scattering contributions of the soil and vegetation components within one resolution cell. Hence, an accurate inversion of soil moisture under vegetation requires the use of additional a priori knowledge on vegetation type and vegetation state (Mattia et al., 2007, Daniel et al., 2009). The fully coherent-on-receive FBD mode of PALSAR aboard the Advanced Land Observing Satellite (ALOS "Daichi") allows the application of partial polarimetric decomposition techniques, and thus has some potential to overcome these limitations for accurate parameter estimation. The aim of this paper is to analyze the potential of PALSAR data collected in the dual polarized FBD343 mode to estimate surface roughness and crop biomass on agricultural fields allowing the correction for the disturbing effects.

* Corresponding author.

2. MATERIALS AND METHODS

2.1 Test Site and In Situ Data

Field measurements were carried out at different test sites within the river Rur catchment, Western Germany. In this paper we only address the arable land test site where ground truth measurements were taken on 6 sampling fields (Fig. 1). The test site Selhausen (50°52'10"N, 6°27'4"E) represents an intensively used agricultural area of the Belgium-Germany loess belt. Crops are grown on virtually flat terrain (slopes from 0-4°, mean elevation approx. 100 m above sea level, mean annual precipitation 705 mm). The dominant soils are Cambisols and Luvisols with a silt loam texture according to the FAO soil classification.

The measurements relevant for the presented study were carried out between July 2007 and October 2009 on land cover types bare soil and sugar beet [*Beta vulgaris* L.]. The size of the individual sampling fields varies between 2 and 10 ha. The surface soil moisture measurements are arranged in a grid with sampling point spacing of 30-60 m, with 12 to 24 points per field. According to the length of the rods of the FDR hand held probes (Theta ML2x Delta-T probes, Delta-T Devices Ltd., Cambridge, UK), the measured surface soil moisture provides an average value for the topmost 6 cm. To minimize sampling errors and to yield representative soil moisture values, each sampling location is represented by the mean of six individual measurements taken within a radius of 40 cm of the sampling location. In total, 120 sampling locations are distributed over the test site.

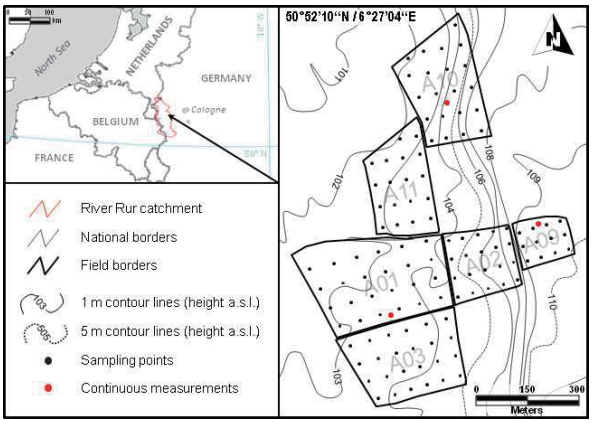

Figure 1. Sampling fields within the arable land test site Selhausen (right)

At the arable land test site, distributed surface soil moisture measurements were carried out for ALOS over-flights on 8/2/2007, 9/17/2007, 5/4/2008, 6/2/2008, and 7/21/2009. In addition, Biomass measurements were carried out every 14 days during the growth periods 2008 and 2009 by harvesting plants at 3 locations. LAI, above- and below-ground biomass, as well as above- and below-ground plant water contents were determined in the laboratory. Furthermore, vegetation height was recorded with each soil moisture measurement in the fields. Measurements of surface roughness were conducted on 5/4/2008, 6/2/2008, and 9/5/2009 using a terrestrial 3D laser scanner (LMS-Z390i, Riegl GmbH, Horn, Austria) and a prototype field laser scanner device (Technology of Crop Farming Institute, University Bonn).

2.2 ALOS PALSAR Data

Table 1: Overview of PALSAR data acquired over the study area and associated field measurements. (m_v, s, and b indicate measurements of soil moisture, RMS height, and biomass)

Date	PALSAR Product	AOI	Track	m_v	s	b
11/28/2006	PSR FBD (dual-pol)	34.3°	647			
8/2/2007	PSR FBD (dual-pol)	34.3°	648	X		
9/17/2007	PSR FBD (dual-pol)	34.3°	648	X		
5/4/2008	PSR FBD (dual-pol)	34.3°	648	X	X	X
6/2/2008	PSR FBD (dual-pol)	34.3°	647	X	X	X
6/19/2008	PSR FBD (dual-pol)	34.3°	648			X
7/18/2008	PSR FBD (dual-pol)	34.3°	647			X
6/22/2009	PSR FBD (dual-pol)	34.3°	648			X
7/21/2009	PSR FBD (dual-pol)	34.3°	647	X		X
9/5/2009	PSR FBD (dual-pol)	34.3°	647		X	X
9/22/2009	PSR FBD (dual-pol)	34.3°	648			X
10/21/2009	PSR FBD (dual-pol)	34.3°	647			

The Phased Array type L-Band Synthetic Aperture Radar (PALSAR) was developed by the Japanese Ministry of Economy, Trade and Industry (METI) as a joint project with the Japan Aerospace Exploration Agency (JAXA). The sensor was launched on January 24, 2006, onboard the ALOS spacecraft. After calibration and validation (Cal/Val), routine operations have been conducted since October 24, 2006. ALOS revolves around the earth in the sun-synchronous orbit of 691.65 km and 98.16 degree inclination resulting in 14 revolutions per day, or once every 100 minutes. The return to the original path (repeat cycle) is every 46 days, and the inner-orbit distance is approximately 59.7 km on the equator.

The SAR data used in this study are 12 PALSAR FBD343 Level 1.1 images acquired in ascending orbit (Table 1). Each of the scenes consists of one horizontally co-polarized (HH) and one fully coherent cross-polarized (HV) Single Look Complex (SLC) image. The incidence angle of the image centre is 34.3 degrees, resulting in a swath width of 70 km. The original slant range resolution is approx. 3 m in azimuth and approx. 15 m in range direction. The radiometric accuracy is better than 0.6 dB (Shimada, 2009).

The schematic processing chain can be seen in figure 2. Multi-looking is executed with a factor of 5:1 (Azimuth/Range) resulting in an image pixel resolution of approx. 15 m. It should be mentioned that, in order to preserve full spatial information, the images are only moderately despeckled using an adaptive Lee-filter with a box-size of 3x3 pixels. Precision terrain correction is carried out using a high resolution (10 m) airborne laser scanner DEM.

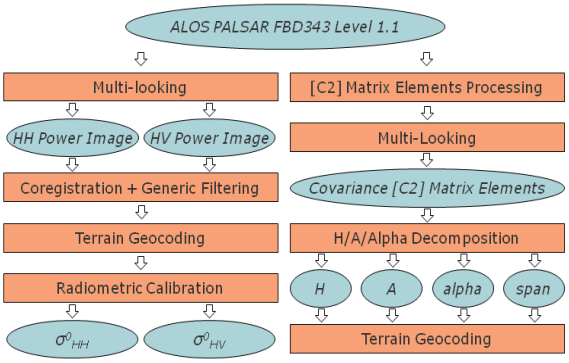

Figure 2. Simplified processing chain for partial polarimetry ALOS PALSAR FBD data

2.3 Dual Polarized H/A/Alpha Decomposition

The dual polarized standard acquisitions (FBD343) of PALSAR aboard "Daichi" provide an additional coherent x-pol channel (HV) allowing the exploitation of the distributed target (2x2) complex Covariance matrix ([C2]) raw binary data off-diagonal elements. The eigenvectors constructed from the [C2] matrix can be used to calculate the dual-pol target parameters entropy (*H*), anisotropy (*A*), and alpha angle (α) by applying the H/A/Alpha Decomposition. The H/A/alpha approach was originally designed to simplify multi-parameter depolarization as occurs for example in quad-pol radar backscatter (Cloude and Pottier, 1996). Cloude (2007) demonstrated that it can also be applied to the simpler case of dual polarization.

As the fully coherent-on-receive FBD mode of ALOS/PALSAR is not capable of reconstructing the complete (3x3) scattering matrix, the dual polarization H/A/Alpha polarimetric decomposition is based on an eigenvector decomposition of the (2x2) complex Covariance [C2] matrix.

$$[C2]=\begin{bmatrix} C_{11} & C_{12} \\ C_{12}^{*} & C_{22} \end{bmatrix} \quad (1)$$

In the dual polarization case the eigenvector decomposition of a distributed target Covariance matrix can be considered as a simple statistical model consisting in the expansion of the (2x2) complex Covariance matrix into a weighted sum of two Covariance matrices.

$$\langle [C2] \rangle = \sum_{i=1}^{2} \lambda_i \underline{v}_i \underline{v}_i^{T*} = \lambda_1 [C2]_1 + \lambda_2 [C2]_2 \quad (2)$$

After this, pseudo-probabilities of the (2x2) complex Covariance [C2] matrix expansion can be defined from the set of sorted eigenvalues.

$$p_i = \frac{\lambda_i}{\sum_{j=1}^{2} \lambda_j} = \frac{\lambda_i}{span} \text{ with } p_1 \geq p_2 \quad (3)$$

The distribution of the probabilities can then be fully described by two parameters. The entropy (H) indicates the degree of statistical disorder of the scattering phenomenon, while for high entropy values (> 0.7), a complementary parameter is necessary to fully characterize the set of probabilities. In this sense, the anisotropy (A) is defined as the relative importance of the secondary scattering mechanism. In the partial polarimetric case, A is equivalent and equal to the wave degree of polarization. It should be mentioned that the condition of mutual orthogonality between the eigenvectors entails that the 2 polarimetric parameters sets resulting from the expansion are not independent.

Each unitary eigenvector of the (2x2) complex Covariance [C2] matrix may be parameterized using 2 real angular variables (Fig. 3).

$$\underline{v}_i = \left[\cos\alpha_i, \sin\alpha_i e^{j\delta_i}\right]^T \quad (4)$$

In the dual polarized case we have a simple interpretation of α on the Poincaré Sphere. The angle α is the angular separation between the received wave polarization state P and the reference state X. In this way, the angles α and δ are indeed related to the orientation and ellipticity angles θ,τ of the received wave's polarization ellipse via a spherical triangle construction on the Poincaré Sphere as shown in figure 3 (Cloude, 2007).

The final products of the polarimetric decomposition are four geocoded images, namely the entropy, anisotropy, alpha angle, and span (Fig. 2, Fig. 7).

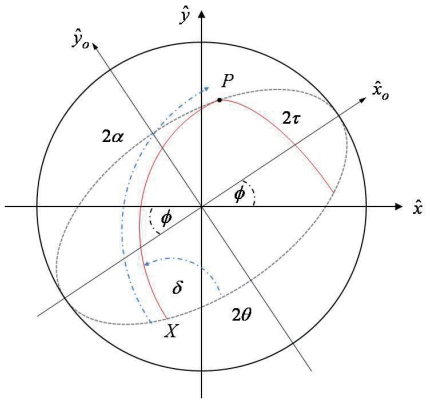

Figure 3: The Poincaré Sphere interpretation of the dual polarization alpha angle

2.4 Comparison of Local Backscattering Signatures with In Situ Data

Based on correlation analysis between the partial polarimetric PALSAR observables and in situ measurements, we investigate the potential to derive information on biomass and surface roughness from the dual-pol entropy, alpha angle, span, and the PALSAR x-pol ratio. Subsequently, we use these to correct the backscatter signal and to devise an improved soil moisture inversion algorithm capable of taking into account the varying vegetation and surface roughness effects.

2.4.1 Sugar Beet Biomass

As mentioned before, sugar beet parameters were monitored on the sampling fields by harvesting 3 to 5 plants at different locations. We assume that the means of the harvested plants at any location represent the mean for the area of the corresponding PALSAR pixel. In regard to interactions with incident EM waves, sugar beet as root crop constitutes a special case compared with other crops (e.g. maize, winter wheat, rape seed, soy beans). Since most of the biomass (and water) is below ground, the above ground vegetation is of minor importance when it comes to the attenuation properties. Indeed, as observed from the field measurements, on sugar beet fields the fruits within the soil can easily hold up to 20 kg/m² of water modulating not only the waves while passing through the canopy, but changing the dielectric constant of the illuminated soil column itself. To account for this effect we use a dedicated sugar beet biomass parameter M_{Beta}. This effective parameter was empirically derived from our dataset with:

$$M_{BETA} = \sqrt{\frac{\left|\sigma_{hv}^{0}\right|^{2}}{\lambda_1 + \lambda_2} \times \overline{\alpha}} \quad (5)$$

The correlation analysis between M_{Beta} and the sum of in situ wet weight above and below ground biomass ($WW_{a.g.}$+$WW_{b.g.}$) yields a highly significant coefficient of determination of 0.64 (Fig. 4).

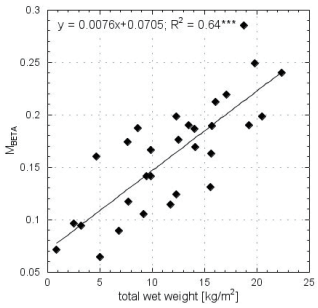

Figure 4: Comparison between effective biomass parameter M_{BETA} and measured total wet weight of sugar beet crops.

2.4.2 Surface Roughness

The roughness was estimated from a 3 dimensional surface model as generated from the terrestrial laser scanner data (Fig. 5). The advantage of this kind of data is the fact that one can easily calculate a sufficient amount of roughness profiles for all possible directions (e.g. perpendicular (PPR) and parallel to the ridges (PAR), perpendicular (PPF) and parallel (PAF) to the flight direction). In this study we use RMS heights averaged from 12 profiles 1 m in length all oriented parallel to the flight direction of Daichi. The area taken into account for each *ks* value equals 8 x 6 PALSAR pixels (approx. 10,800 m²).

Figure 5: Terrestrial laser scanner 3D composite image of field A01 on May 4, 2008. (Courtesy D. Hoffmeister)

The mean RMS height s_{PAF} perpendicular to the incident EM waves is then defined as:

$$s_{PAF} = \sqrt{\frac{\sum_{i=1}^{n}\left(z_i - \bar{z}\right)^2}{n-1}} \qquad (6)$$

Since the roughness term in radar science is a function of wavelength, its appearance changes with different frequencies. That is, at lower frequencies, the surface of an illuminated target appears smoother than at higher frequencies. To compensate this effect, the RMS height is scaled to the actual wavelength using the wavenumber *k* with the following equation:

$$ks = s_{PAF} \times \frac{2\pi}{\lambda} \qquad (7)$$

where *ks* is the RMS height normalized to the PALSAR wavelength λ of 23.62 cm.

The mean *s* values calculated from the PAF profiles ranged from 0.51 to 3.37 cm resulting in *ks* values from 0.14 to 0.93. The very smooth state with *ks* values < 0.2 was recorded after an intense precipitation event one month after seeding.

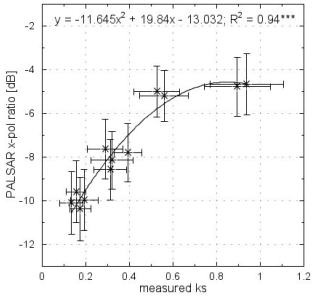

Figure 6: Comparison between PALSAR x-pol (HV/HH) ratio and measured surface roughness *ks*.

A coefficient of determination of 0.94 for the comparison between measured *ks* and the corresponding backscattering signature indicates that the PALSAR HV/HH ratio [dB] is highly sensitive to surface roughness (Fig. 6).

3. RESULTS AND DISCUSSION

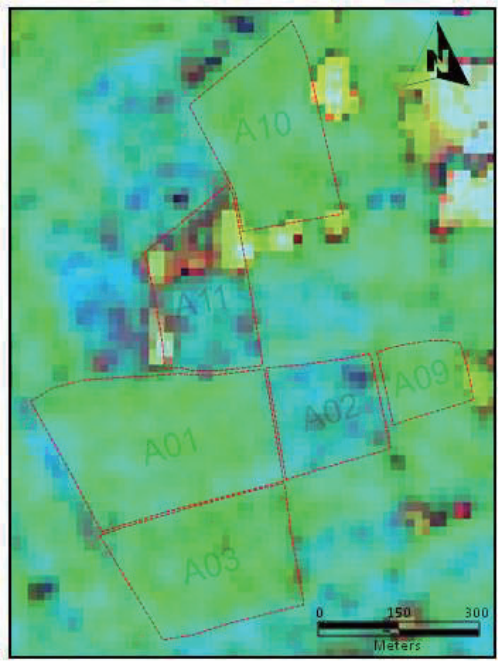

Figure 7: HSV image of the Selhausen test site from 21st July 2009. (Hue = Alpha, Saturation = Entropy, Value = Span)

In order to view the products of the polarimetric decomposition, we employ a HSV colour-coding scheme with the hue equal to the alpha angle. The entropy is used as saturation term, so the colour saturation decreases with increasing entropy. The scattered total power is employed to modulate the intensity through the value term. Figure 7 shows how the sampling fields have different signature in the entropy/alpha domain on July 21, 2010. We note significant variation of scattering behaviour from the various land cover types indicating the potential of discrimination and classification based on the dual-pol phase information. The green colour represents low or no vegetation. Sugar beet fields and tree hedges appear bluish, while the maize in the northern part of field A11 is going into reddish. The very bright areas in the eastern part represent double bounce effects from man made structures.

3.1 Biomass Estimation

As already mentioned in the section before, we empirically derived (5) as effective biomass parameter from our extensive data set. The highly significant correlation between in situ total wet weight and M_{BETA} indicate the potential of the introduced parameter. Using the relationship found from the correlation analysis between polarimetric PALSAR parameter M_{BETA} and in situ sugar beet biomass, we can estimate above and below ground wet weight of the crops with:

$$WW_{a.g.+b.g.} = 83.747\left(\sqrt{\frac{\sigma^0_{hv}}{\lambda_1+\lambda_2}\times\bar{\alpha}}\right) - 1.599 \qquad (8)$$

A comparison between measured and estimated total wet weight yields an RMS error of 2.661 kg/m² as can be seen in figure 8. It should be noted that the biomass estimates are well aligned along the ± 2 kg error line.

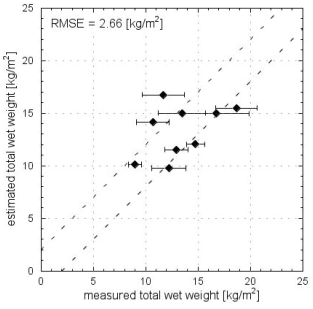

Figure 8: Estimated versus measured total wet weight of sugar beet crops. The bars represent the standard error of the plant samples.

3.2 Surface Roughness Estimation

Four different agricultural soil surface states could be identified from the in situ measurements: very smooth, seeded, harrowed, and deeply ploughed. We estimate the surface roughness from the polarimetric PALSAR data based on the found relationship between *ks* and the cross-pol ratio with:

$$ks = 0.0157\left(\frac{\sigma^0_{hv}}{\sigma^0_{hh}}\right)^2 + 0.3452\left(\frac{\sigma^0_{hv}}{\sigma^0_{hh}}\right) + 2.0634 \qquad (9)$$

Figure 9 shows the comparison between estimated and measured *ks* values. We retrieve *ks* from the dual polarized PALSAR data with a RMS error of 0.11. It can be seen that the estimates are well distributed along the zero error line.

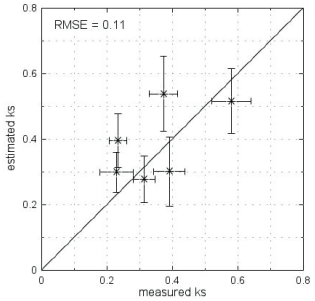

Figure 9: Estimated versus measured surface roughness. The bars represent the standard errors.

3.3 Soil Moisture Estimation

Subsequently, the estimates of *ks* and biomass can be used to correct for their influence on the PALSAR backscattering coefficient. A first test is carried out based on a simple empirical bare soil relationship between volumetric soil moisture m_v and the horizontally polarized transmit, horizontally polarized receive (HH) case (11). We use the derived roughness information to correct sigma nought with:

$$\sigma^0_{hh}{}' = \left(\sigma^0_{hh}\right)\times ks^{ks} \qquad (10)$$

Then m_v is calculated with:

$$m_v = -0.625\left(\sigma^0_{hh}{}'[dB]\right)^2 - 20.128\left(\sigma^0_{hh}{}'[dB]\right) - 132.11 \qquad (11)$$

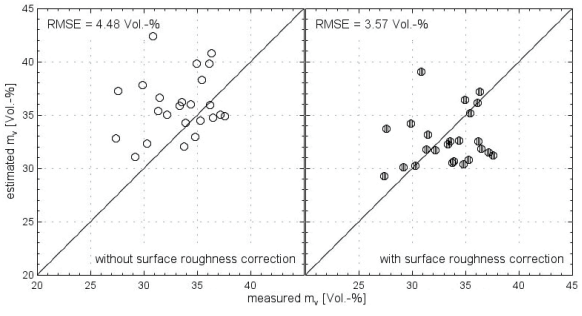

Figure 10: Estimated versus measured soil moisture (left: without roughness correction; right: with roughness correction)

The comparison between estimated and measured m_v shows that the RMS error is 4.48 Vol.-% for the backscatter coefficients without roughness correction and 3.57 Vol.-% for the backscatter coefficients with roughness correction (Fig. 10). It is obvious that the estimates are distributed much closer to the zero error line after the surface roughness correction.

It should be mentioned that in the foregoing section we presented first results from the ongoing research. The accuracy estimations are preliminary. All validation data have not been used in the correlation analyses before, and thus is considered to be fully independent.

4. CONCLUSIONS

In this paper we have introduced a novel approach to develop an empirical soil moisture algorithm for dual-polarized PALSAR data. In particular the dual-pol H/A/Alpha decomposition was applied to exploit the polarimetric phase information contained in the FBD343 mode. Our first results show the great potential of the applied method to directly invert biomass and surface roughness information from the partial polarimetric L-band data. Along with the land-use classification capabilities of dual-polarized L-band SAR systems (Lee et al., 2001), the findings give a promising outlook in terms of the possibility to develop a really operational soil moisture retrieval model for PALSAR data collected in the FBD mode. That is, information on the land cover and the disturbing effects from vegetation and surface roughness can be derived without the use of a priori knowledge or auxiliary EO data. The next step in the ongoing research will be the application of the technique to crop types cereals, maize, and rapeseed, as well as for land cover type grassland.

ACKNOWLEDGEMENTS

The authors thank the Japan Aerospace Exploration Agency (JAXA) and the European Space Agency (ESA) for the provision of ALOS PALSAR data through their PI programme (AOALO.3570). We gratefully acknowledge financial support by the SFB/TR-32 "Pattern in Soil-Vegetation-Atmosphere Systems: Monitoring, Modelling, and Data Assimilation" funded by the German Research Foundation (DFG). Our thanks also go to Dirk Hoffmeister and Marin Dimtrov for the 3D laser scanner data, as well as to the farmers, who made their fields available to us.

REFERENCES

Cloude, S.R. and E. Pottier, 1996. A Review of Target Decomposition Theorems in Radar Polarimetry. *IEEE TGRS*, 34(2), pp. 498-518.

Cloude, S.R., 2007. The Dual Polarisation Entropy/Alpha Decomposition: A PALSAR Case Study. In *Proc. of 3rd Int. Workshop on Science and Applications of SAR Polarimetry and Polarimetric Interferometry*, *PolInSAR 2007*; 22-26 January 2007, ESA-ESRIN, Frascati, Italy.

Daniel, S., S. Allain, L. Ferro-Famil, and E. Pottier, 2009. Soil Moisture Retrieval Over Periodic Rough Surfaces Using PolSAR Data. In *Proc. of 4th Int. Workshop on Science and Applications of SAR Polarimetry and Polarimetric Interferometry*, *PolInSAR 2009*; 26-30 January 2009, ESA-ESRIN, Frascati, Italy.

Lee, J.S., M.R. Grunes, and E. Pottier, 2001. Quantitative Comparison of Classification Capability: Fully Polarimetric Versus Dual and Single-Polarization SAR. *IEEE TGRS*, 39(11), pp. 2343-2351.

Mattia, F., G. Satalino, A. Balenzano, V.R.N. Pauwels, N.E.C. Verhoest, H. Skriver, and M. Davidson, 2007. Exploiting L-band SAR data for the improvement of surface process modelling. In *Proc. of 5th Int. ESA Symp. on Retrieval of Bio- and Geophysical Parameters from SAR Data for Land Applications*, Bari, Italy, 25-28 September.

Nord, M.E., T.L. Ainsworth, J.S. Lee, and N.J.S. Stacy, 2009. Comparison of Compact Polarimetric Synthetic Aperture Radar Modes. *IEEE TGRS*, 47(1), pp. 174-188.

Shimada, M., 2009. PALSAR Polarimetric Accuracy and Stability Evaluated for Three Years Amazon Data. In *Proc. of 4th Int. Workshop on Science and Applications of SAR Polarimetry and Polarimetric Interferometry*, *PolInSAR 2009*; 26-30 January 2009, ESA-ESRIN, Frascati, Italy.